Effect of the Wall Thickness of the Vessel on FFR$_{CT}$ of Carotid Artery Stenosis

Long Yu[1], Kesong Xu[1], Jun Wan[2], Haiyan Lu[3, *] and Shengzhang Wang[1, *]

Abstract: Fractional flow reserve (FFR) computed from computed tomography angiography (CTA), i.e., FFR$_{CT}$ has been used in the clinic as a noninvasive parameter for functional assessment of coronary artery stenosis. It has also been suggested to be used in the assessment of carotid artery stenosis. The wall thickness of the vessel is an important parameter when establishing a fluid-structure coupling model of carotid stenosis. This work studies the effect of the vessel wall thickness on hemodynamic parameters such as FFR$_{CT}$ in carotid stenosis. Models of carotid stenosis are established based on CTA image data using computer-aided design software. It is assumed that the vessel wall is a linear elastic and isotropic material, and the blood an incompressible Newtonian fluid. Under the pulsating flow condition, ANSYS Transient Structural and CFX are used to simulate the blood flow of fluid-structure coupling in the carotid stenosis model in order to obtain hemodynamic parameters and the corresponding FFR$_{CT}$. The results show that when the elastic modulus of the vessel wall is fixed, FFR$_{CT}$ will decrease with the increase of the wall thickness. Similarly, FFR$_{CT}$ will decrease with the increase of the elastic modulus when the wall thickness is fixed. The difference in hemodynamic parameters such as FFR$_{CT}$, however, is relatively small if the stiffness of the two models are close. The results demonstrate that the effect of the vessel wall thickness, especially for a model with small elastic modulus, should be taken into account in using FFR$_{CT}$ for functional assessment of carotid stenosis. Moreover, under the linear elasticity and isotropic material assumptions, the stiffness coefficient may replace the elastic modulus and wall thickness as a parameter reflecting material property of the vessel wall in the carotid stenosis model.

Keywords: Carotid artery stenosis, fractional flow reserve, fluid-structure coupling, numerical simulation, stiffness coefficient.

1 Introduction

Fractional flow reserve (FFR) is a quantitative index used to evaluate the degree of coronary artery stenosis [Taylor, Fonte and Min (2013); Xie, Zheng, Duan et al. (2017)].

---

[1] Institute of Biomechanics, Department of Aeronautics and Astronautics, Fudan University, Shanghai, China.

[2] Interventional Department, Shanghai Jing'an District Central Hospital, Shanghai, China.

[3] Interventional Ultrasound Division of VIP Clinic Department, Dongfang Hospital Affiliated to Tongji University, Shanghai, China.

[*] Corresponding Authors: Shengzhang Wang. Email: szwang@fudan.edu.cn;
  Haiyan Lu. Email: lhy.wf@163.com.

It is calculated by the ratio of downstream to upstream pressure of the vascular stenosis when the peripheral vessels reach the maximum diastolic state under the drug induction [Pijls, Van Son, Kirkeeide et al. (1993)]. However, FFR measured by pressure wire in clinical application is limited by the following disadvantages: (a) difficult to deliver pressure wire to the distal end of the coronary artery and having risk of interfering with lesions and damaging blood vessels; (b) high cost of the pressure wire; (c) easy to cause adverse reactions in patients during measurements. Therefore, many researchers have managed to combine computational fluid dynamics with CTA image data to calculate FFR through mechanical modeling and numerical simulation. In addition to coronary artery stenosis, carotid artery stenosis is currently one of the most dangerous vascular diseases [Fan, Liu, Sun et al. (2017); Jin and Qiao (2016); Zhang (2015)], particularly the internal carotid artery stenosis which may cause cerebral ischemia or even cerebral infarction. At present, the evaluation of the degree of carotid stenosis is still based on the stenosis rate in clinic [Augst, Barratt, Hughes et al. (2003); Yu, Li, Li et al. (2018)], but the stenosis rate is purely dependent on image data with a low accuracy of functional stenosis evaluation. In order to increase the accuracy of the assessment of carotid stenosis, some scholars have tried to introduce FFR_{CT} into the evaluation of carotid stenosis, while many of them using assumptions of the rigid wall of the carotid vessel. Our group takes the assumption of linear elasticity for the elastic vessel wall, hoping to obtain a more accurate FFR_{CT} which provides a foundation for the functional assessment of carotid stenosis [Huang, Zhu, Zhou et al. (2015)].

We have previously discussed the effects of the elastic modulus of the vessel wall and the plaque on the calculation of FFR_{CT}. The results indicate that the elastic modulus of the vessel wall has a significant effect, while the elastic modulus of the plaque affects little [Yu, Xu, Wan et al. (2019a); Yu, Xu, Wan et al. (2019b)]. However, our previous models used vessel walls with a thickness of 0.5 mm, which may be inconsistent with the real situation [Song (2015)]. Based on our previous studies, this paper establishes a carotid artery stenosis model with different wall thicknesses reconstructed from CTA image data, numerical simulates the blood flow, and discusses the influence of the vessel wall thickness on FFR_{CT}.

2 Method

2.1 Geometry modeling

The CTA data were imported into Mimics 17.0 (Materialise, Belgium) to reconstruct a 3D geometric model. The 3D model will be imported into Geomagic Studio 11.0 (Geomagic, USA) for Boolean operation to obtain a model of carotid artery stenosis. The stenosis rate of the carotid artery we construct is 76.53%. We took the assumption that the vessel wall is linear elastic and isotropic, and then set the density of the vessel wall at 1150 kg/m³, Poison's ratio at 0.45 [Qian, Zhang, Wang et al. (2010)] in ANSYS Transient Structural 18.2 (ANSYS, USA). Parameters of the vessels and blood are obtained from the literature. The effect of the residual stress in the vessel wall is very important in the fluid-structure coupling simulation of vessels which may affect the deformation of the blood vessel wall and thus affect the flow field, but it is difficult to obtain patient-specific residual stress distribution with current techniques. Besides, our work aims to use the coefficient FFR_{CT} obtained by fast and economical CTA imaging to assess the functional stenosis of the carotid artery, so the assumption that there is no residual stress of the vessel wall is

acceptable. The material property of plaque was fixed the same as that of the vessel wall due to our previous studies. A group of numerical models were established from the same clinically geometric model of carotid artery stenosis. The elastic modulus of the group was fixed at 0.8 MPa, while the thickness of the vessel wall was set from 0.5 mm to 1.0 mm. [Wang (2007); Wang, Wang, Wu et al. (2005)].

2.2 Meshing

The fluid and solid domains were meshed using ANSYS ICEM CFD (ANSYS, USA). The fluid boundary layer was a five-layer triangular prism grid, and the elements were internal tetrahedral. Taking into account the presence of the plaque, the tetrahedral elements were used to mesh the solid domain. In addition, for grids with different sizes, we tested the dependence of the grids by the total energy loss from the inlet to the outlet. Take the model with a wall thickness of 0.5 mm and an elastic modulus of 0.8 MPa for instance, when the maximum grid size of the solid domain was less than 0.4 mm and that of the fluid domain was less than 0.5 mm, the energy loss per unit volume of the model was less than 1% at the convergent results. Therefore, the maximum size of the solid domain elements was set at 0.4 mm, and 0.5mm in the fluid domain. A total of 37,433 nodes and 122,573 elements was meshed for the fluid domain and a total of 21,348 nodes and 85,776 elements for the solid domain.

2.3 Blood parameters

Blood is non-Newtonian in reality, but according to the researches of Aenis et al. [Aenis, Stancampiano, Wakhloo et al. (1997)], when the vessel diameter was larger than 0.5 mm, the calculation error replacing Newton fluid with non-Newtonian fluid was less than 2%. For the model we built had a diameter much larger than 0.5 mm, we set the blood in ANSYS CFX 18.2 as the incompressible Newtonian fluid with a density of 1060 kg/m^3 and a viscosity of 0.0039 Pa· s [Qian, Zhang, Wang et al. (2010); Tao (2014)]. In the whole calculation process, the maximum Reynolds number was about 1698, so the blood flow in this model could be presumed as laminar flow.

2.4 Governing equations and boundary conditions

In the fluid-structure coupled model of carotid artery stenosis, the blood flow control equation could be described as follows:

$$\nabla \cdot u = 0 \tag{1}$$

$$\rho \left(\frac{\partial u}{\partial t} + (u \cdot \nabla)u \right) = -\nabla p + \nabla \cdot \boldsymbol{\tau} \tag{2}$$

where u is the velocity vector; p is the flow field pressure, ρ is the blood density, and $\boldsymbol{\tau}$ is the stress tensor. The governing equation of the vascular wall is

$$\rho_s \, a_s = \nabla \cdot \boldsymbol{\sigma_s} \tag{3}$$

In the above equation, ρ_s is the density of blood vessels, a_s is the vascular wall particle acceleration, and $\boldsymbol{\sigma_s}$ is the vascular wall stress tensor [Liu, Yin, Zhang et al. (2015)]. We conducted two-way coupled fluid-structure simulation which solved the fluid and solid domain separately at each time step and then transferred the data of displacement and

pressure between two parts on the interface automatically by ANSYS Transient Structural and CFX.

The boundary conditions on the vessel wall were all fixed with six degrees of freedom on the inlet and two outlet surfaces, and the inner surface of the vessel wall was set as the fluid-structure interaction surface. The boundary conditions of the fluid were velocity boundary condition at the inlet, open pressure boundary conditions at the two outlets and no-slip condition at the wall [Grinberg, Yakhot and Karniadakis (2009); Idzenga, Reesink, van Swelm et al. (2012)]. The velocity waveform at the inlet and pressure waveform at the outlet were obtained by fitting the velocity waveform of the common carotid artery (measured by ultrasonic Doppler measuring) and the pressure waveform of the carotid artery, as shown in Fig. 1 [Holdsworth, Norley, Frayne et al. (1999); Karimpour and Javdan (2014); Meinders and Hoeks (2004)].
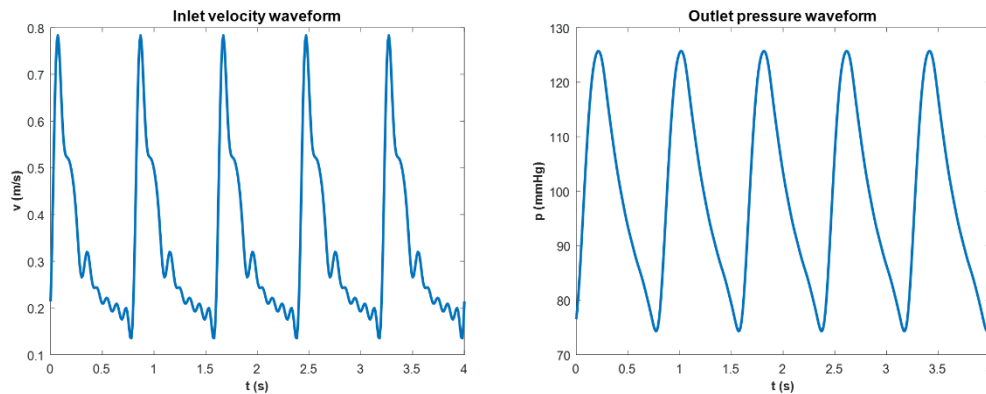

Figure 1: Inlet velocity waveform and outlet pressure waveform

2.5 Simulation settings

In order to eliminate the influence of the initial conditions, the total solution time was set as 4.08 s for five cardiac cycles with the same waveforms, and the time step was set at 0.008 s. For each time step, when the iteration error was less than 1×10^{-4}, the calculation result was considered to be convergent. The results converged at the forth cardiac cycle, so the results of the fifth cardiac cycle were chosen to analyze the hemodynamic parameters, such as the flow velocity, pressure, FFR_{CT}, wall shear stress, etc. when the vessel reached the maximum filling state at the peak systolic (4.072 s). FFR_{CT} was calculated by the pressure at the outlet of the internal carotid artery divided by the pressure at the outlet of the common carotid artery.

3 Results

When the elastic modulus of the vessel wall was fixed at 0.8 MPa, a third-order polynomial was used to fit FFR_{CT} data corresponding to different wall thicknesses, as shown in Fig. 2. With the wall thickness increasing from 0.5 mm to 1.0 mm, FFR_{CT} decreased from 0.8156 to 0.7529. When the wall thickness reached 0.9 mm and increased to larger, FFR_{CT} almost stayed unchanged. Taking FFR_{CT} with 0.5 mm wall thickness as the reference value (0.8156),

we found that FFR$_{CT}$ decreased by 4.2% from the wall thickness of 0.5 mm to 0.6 mm. While from 0.8 mm to 0.9 mm, it decreased by 0.5%. The relative difference of FFR$_{CT}$ could be calculated by the fitting formula and described as follows: when the wall thickness was less than 0.55 mm, it was less than 2%; when the wall thickness was less than 0.65 mm, it was less than 5%. All the FFR$_{CT}$ calculated in the research were listed in Tab. 1.
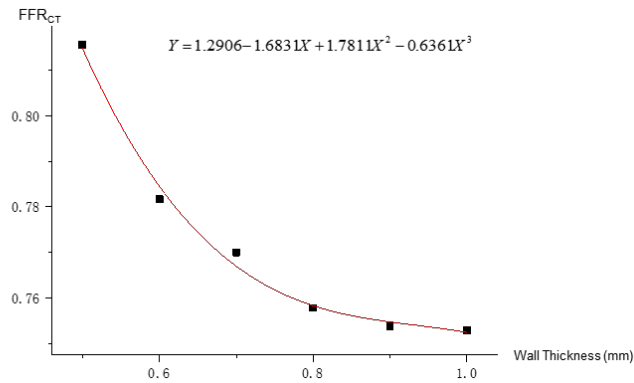

$$Y = 1.2906 - 1.6831X + 1.7811X^2 - 0.6361X^3$$

Figure 2: Relationship between FFF$_{CT}$ and the wall thickness when fixing the elastic modulus

Table 1: Relationship between intravascular pressure and wall thickness at fixed elastic modulus

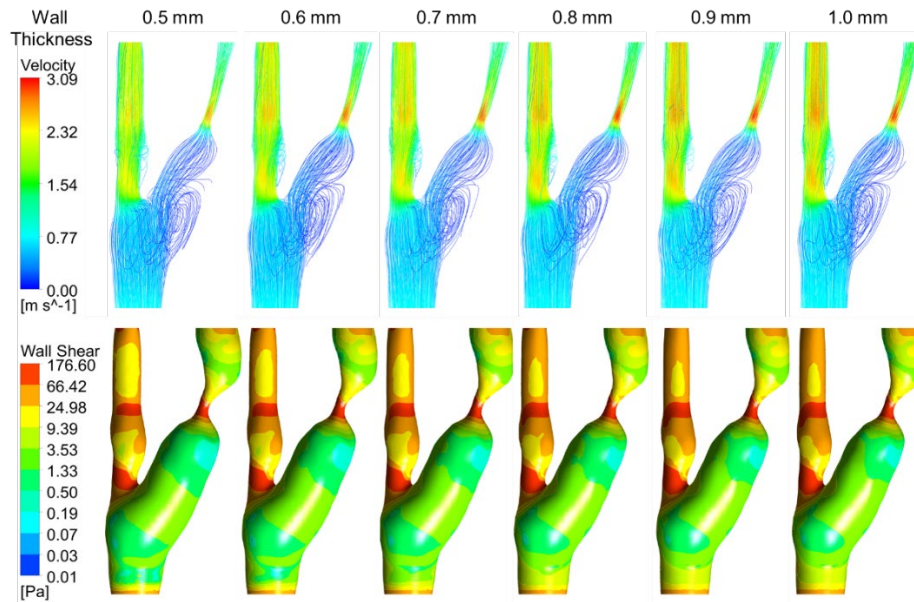| Wall Thickness (mm)	Pressure at internal carotid artery (Pa)	Pressure at external carotid artery (Pa)	FFR$_{CT}$
0.5	13034.0	16020.3	0.8136
0.6	13019.5	16666.0	0.7812
0.7	13019.5	17522.3	0.7430
0.8	13018.8	17179.6	0.7578
0.9	13018.9	17288.7	0.7530
1.0	13018.9	17242.4	0.7551

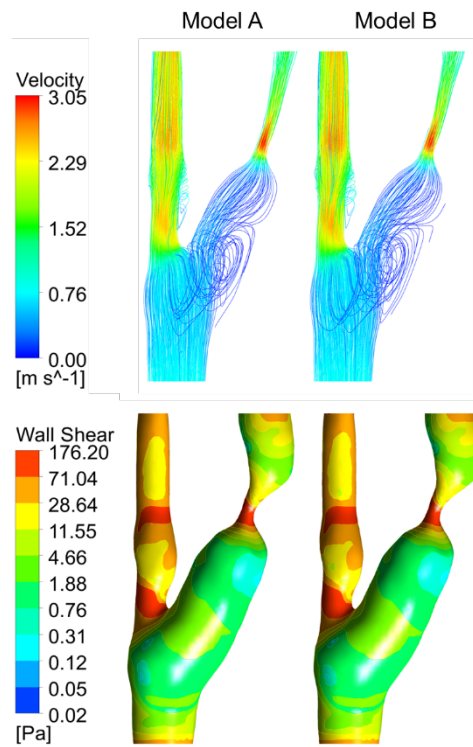**Figure 3:** Streamline and wall shear stress for different wall thicknesses

Fig. 3 presented the streamlines and the wall shear stresses of the models with a fixed elastic modulus at 0.8 MPa and different vessel wall thicknesses. When the vessel wall thickness increased from 0.5 mm to 1.0 mm, the maximum velocity increased from 2.73 m/s to 3.09 m/s and the maximum wall shear stress increased from 143.4 Pa to 176.6 Pa. Taking the maximum velocity and the maximum wall shear stress with 0.5 mm wall thickness as the reference value, we found that (a) when the wall thickness increased from 0.5 mm to 0.7 mm, the maximum velocity increased by 0.22 m/s, 8.1% relative to the reference value and the maximum wall shear stress increased by 25.1 Pa, 17.5% relative to the reference value; (b) when the wall thickness increased from 0.8 mm to 1.0 mm, the maximum velocity increased by 0.04 m/s, 1.5% relative to the reference value and the maximum wall shear stress increased by 0.4 Pa, 0.3% relative to the reference value; (c) when the wall thickness increased from 0.5 mm to 1.0 mm, the maximum velocity increased significantly as the streamlines displayed and the region area of high wall shear stress (greater than 25 Pa) increased significantly.

Discuss two models from the above results: A) the model of a wall thickness of 0.8 mm and the elastic modulus of 0.8 MPa; B) the model of a wall thickness of 0.5 mm and the elastic modulus of 1.2 MPa. The hemodynamic parameters of the two models are listed in Tab. 2.

Table 2: Hemodynamic parameters for Model A and B

	Model A	Model B	Difference (%)
FFR$_{CT}$	0.7578	0.7582	0.05
Maximum flow velocity	3.048 m/s	3.041 m/s	0.23
Maximum wall shear stress	176.2 Pa	172.5 Pa	2.09

The streamlines of the two models were compared as well as the wall shear stress diagrams, as shown in Fig. 4. There was no significant difference between the flow field and the wall shear stress distribution. If the product of the elastic modulus and the wall thickness was defined as the stiffness coefficient, it could be found that the stiffness coefficient of the Model A was 0.64, and that of the model B was 0.60, i.e., the stiffness coefficient of the two models was very close, similar to the hemodynamic parameters of the two models.

Figure 4: Streamline and wall shear stress for models with similar FFR$_{CT}$

4 Discussion

When keeping the elastic modulus of the vessel wall fixed, FFR$_{CT}$ decreased monotonously with the increase of the wall thickness, while the maximum blood flow velocity and wall

shear stress increased, indicating that the wall thickness should be considered in the numerical simulation of models with elastic walls.

When the wall thickness is fixed, as we discussed in our previous research [Yu, Xu, Wan et al. (2019a)], FFR_{CT} decreased monotonously with the increase of elastic modulus of the vessel wall, while the blood flow velocity and maximum wall shear stress increased.

It was found that FFR_{CT} calculated differed little with different wall thicknesses or elastic modulus for the two models with approximate stiffness coefficients. Moreover, the maximum velocity and the maximum wall shear stress were nearly equal with no significant difference in the distribution of streamlines and high wall shear stress regions. In the follow-up study, we would further conduct the effect of the stiffness coefficient on numerical simulation results.

This study also has some limitations, e.g., the two outlets pressure was set the same in the fluid domain, contradictory to the fact that the pressure at different outlets are determined by the resistance of the downstream vessels. In the follow-up study, we would use ultrasound to measure the flows at two outlets and convert it into pressure boundary conditions at the outlet, expecting for more accurate calculation results [Ohsaki, Miyamura and Zhang (2016); Zhang, Fan, Dong et al. (2016)]. Anisotropic hyper-elastic materials will also replace isotropic linear elastic assumptions in the next study to obtain a model closer to the true constitutive vascular structure. Due to the difficulty in obtaining the specificity of the wall residual stress of each patient's, this study has not examined the effect of the wall residual stress on the numerical calculation [Yang, Zhang, Hua et al. (2018)]. In the next study, we will consider it and analyze the result difference between considering wall residual stress or not.

5 Conclusion

When establishing the fluid-structure coupling model of carotid artery stenosis, the changes in the wall thickness would result in the changes of FFR_{CT}, and FFR_{CT} calculated has a significant difference when the elastic modulus is small. There are negligible differences, however, in the FFR_{CT} calculated, the flow field distribution and the wall shear stress distribution when the stiffness coefficients of the vascular walls are relatively close. Therefore, in the fluid-structure coupling model of carotid artery stenosis, under the assumption of linear elasticity and isotropic, the stiffness coefficient of the vessel wall can be taken as a parameter reflecting the property of it.

References

Aenis, M.; Stancampiano, A. P.; Wakhloo, A. K.; Lieber, B. B. (1997): Modeling of flow in a straight stented and nonstented side wall aneurysm model. *Journal of Biomechanical Engineering*, vol. 119, no. 2, pp. 206-212.

Augst, A. D.; Barratt, D. C.; Hughes, A. D.; Glor, F. P.; McG, S. T. et al. (2003): Accuracy and reproducibility of CFD predicted wall shear stress using 3D ultrasound images. *Journal of Biomechanical Engineering*, vol. 125, no. 2, pp. 218-222.

Fan, Z. M.; Liu, X.; Sun, A. Q.; Zhang, N.; Fan, Z. M. et al. (2017): Noninvasive functional assessment of internal carotid artery stenosis using CT angiography. *Journal of Medical Biomechanics*, vol. 32, no. 1, pp. 32-37.

Grinberg, L.; Yakhot, A.; Karniadakis, G. E. (2009): Analyzing transient turbulence in a stenosed carotid artery by proper orthogonal decomposition. *Annals of Biomedical Engineering*, vol. 37, no. 11, pp. 2200-2217.

Holdsworth, D. W.; Norley, C. J. D.; Frayne, R.; Steinman, D. A.; Rutt, B. K. (1999): Characterization of common carotid artery blood-flow waveforms in normal human subjects. *Physiological Measurement*, vol. 20, no. 3, pp. 219.

Huang, J. L.; Zhu, Y. J.; Zhou, F. Y.; Gu, W. J.; Zhang, L. et al. (2015): Effects of inflation pressures on mechanical environment in carotid after stent implantation by numerical simulation. *Journal of Interventional Radiology*, vol. 24, no. 12, pp. 1106-1109.

Idzenga, T.; Reesink, K. D.; van Swelm, Y.; Hansen, H. H.; Holewijn, S. et al. (2012): Noninvasive estimation of the blood pressure waveform in the carotid artery using continuous finger blood pressure monitoring. *Ultrasound in Medicine & Biology*, vol. 38, no. 11, pp. 1998-2006.

Jin, L.; Qiao, A. K. (2016): Biomechanical mechanism and quantitative assessment indices for vulnerable carotid plaques. *Journal of Medical Biomechanics*, vol. 31, no. 1, pp. 464-468.

Karimpour, H.; Javdan, E. (2014): Simulation of stenosis growth in the carotid artery by lattice boltzmann method. *Journal of Mechanics in Medicine and Biology*, vol. 14, no. 2, pp. 1450016.

Liu, Y.; Yin, Y. F.; Zhang, D. F.; Zhang, Z. L. (2015): Analysis of non-newtonian blood flow in stenotic carotid artery under fluid-structure interaction. *Applied Mathematics and Mechanics*, vol. 36, no. 10, pp. 1058-1066.

Meinders, J. M.; Hoeks, A. P. (2004): Simultaneous assessment of diameter and pressure waveforms in the carotid artery. *Ultrasound in Medicine & Biology*, vol. 30, no. 2, pp. 147-154.

Ohsaki, M.; Miyamura, T.; Zhang, J. Y. (2016): A piecewise linear isotropic-kinematic hardening model with semi-implicit rules for cyclic loading and its parameter identification. *Computer Modeling in Engineering & Sciences*, vol. 111, no. 4, pp. 303-333.

Pijls, N. H.; Van Son, J. A.; Kirkeeide, R. L.; De Bruyne, B. L. G. K.; Gould, K. L. (1993): Experimental basis of determining maximum coronary, myocardial, and collateral blood flow by pressure measurements for assessing functional stenosis severity before and after percutaneous transluminal coronary angioplasty. *Circulation*, vol. 87, no. 4, pp. 1354-1367.

Qian, X. Q.; Zhang, X. H.; Wang, Y.; Li, Y.; Liu, Z. C. (2010): Fluid-solid coupling analysis of the coronary artery based on the CT images. *Beijing Biomedical Engineering*, vol. 29, no. 4, pp. 331-335.

Song, D. X. (2015): *Mechanics of Atherosclerosis Index (Ph.D. Thesis).* University of Yanshan, China.

Tao, J. (2014): *Hemodynamic Numerical Simulation of before and after Carotid Artery Stenting on Carotid Artery Stenosis (Ph.D. Thesis).* University of Dalian Medical, China.

Taylor, C. A.; Fonte, T. A.; Min, J. K. (2013): Computational fluid dynamics applied to cardiac computed tomography for noninvasive quantification of fractional flow reserve: scientific basis. *Journal of the American College of Cardiology*, vol. 61, no. 22, pp. 2233-2241.

Wang, J. C. (2007): *Experimental and Clinical Studies on Quantitative Evaluation of Common Carotid Artery Elasticity with E-Tracking Technique (Ph.D. Thesis).* University of Heibei Medical, China.

Wang, J. H.; Wang, Y. H.; Wu, C. L.; Du, X.; Zhang, L. et al. (2005): Quantitative evaluation of carotid elasticity in normal adults by echo tracking technique. *Chinese Journal of Ultrasonography*, vol. 14, no. 4, pp. 292-294.

Xie, X.; Zheng, M.; Duan, X.; Xie, S.; Wang, Y. (2017): Direct coronary coupling approach for computing FFR_CT. *Journal of Mechanics in Medicine and Biology*, vol. 17, no. 3, 1750043.

Yang, S.; Zhang, L. T.; Hua, C.; Liu, Y.; Tang, J. et al. (2018): A Prediction of *in vivo* mechanical stresses in blood vessels using thermal expansion method and its application to hypertension and vascular stenosis. *Acta Mechanica Sinica*, vol. 34, no. 6, pp. 1156-1166.

Yu, L.; Xu, K. S.; Wan, J.; Wang, S. Z.; Lu, H. Y. (2019): The effect of elastic modulus of vessel on FFR_{CT} of carotid artery stenosis. *Journal of Mechanics in Medicine and Biology* (Accepted).

Yu, L.; Xu, K. S.; Wan, J.; Wang, S. Z. (2019): The influence of the elastic modulus of the plaque in carotid artery on the computed results of FFR_{CT}. *Computer Methods in Biomechanics and Biomedical Engineering* (Submitted).

Yu, M. M.; Li, Y. H.; Li, W. B.; Lu, Z. G.; Wei, M. et al. (2018): Diagnostic performance of machine learning based FFR_{CT} in coronary artery stenosis**.** *International Journal of Medical Radiology*, vol. 41, no. 3, pp. 282-286.

Zhang, D. F. (2015): *Research on Hemodynamics of Atherosclerotic Plaque Formation and in-Stent Restenosis in Carotid Artery (Ph.D. Thesis).* University of Nanchang, China.

Zhang, Y.; Fan, Q.; Dong, L.; Atluri, S. N. (2016): Are "higher-order" and "layer-wise zig-zag" plate & shell theories necessary for functionally graded materials and structures? *Computer Modeling in Engineering & Sciences*, vol. 112, no. 1, pp. 1-32.